



# TEM study on the electrical discharge machined surface of single-crystal silicon

J.W. Murray<sup>a</sup>, M.W. Fay<sup>b</sup>, M. Kunieda<sup>c</sup>, A.T. Clare<sup>a,\*</sup>

<sup>a</sup> Precision Manufacturing Centre, Department of Mechanical, Materials and Manufacturing Engineering, University of Nottingham, University Park, Nottingham NG7 2RD, UK

<sup>b</sup> Department of Physics and Astronomy, University of Nottingham, University Park, Nottingham NG7 2RD, UK

<sup>c</sup> Department of Precision Engineering, The University of Tokyo, Tokyo, Japan

## ARTICLE INFO

### Article history:

Received 12 September 2012

Accepted 27 November 2012

Available online 7 December 2012

### Keywords:

EDM  
Single crystal silicon  
TEM  
Raman  
Deposition  
Recast layer

## ABSTRACT

EDM is a useful process for machining high-aspect ratio features with good accuracy in electrically conductive materials irrespective of their mechanical properties. With the ability of micro-EDM to compete with the resolution of conventional semi-conductor processing techniques, the process has attracted interest for the potential machining of single-crystal silicon. In order for the process to be feasible, the damage mechanism occurring during machining must be characterised to assess the need for secondary processing. Despite this the microstructural transformations induced by the process on the surface of the workpiece have not yet been assessed. In this study transmission electron microscopy (TEM) and laser-Raman spectroscopy are employed to characterise the microstructural changes as well as the presence of any contaminants and defects at the nano-scale. A twinned-crystalline structure created by epitaxial growth is formed in the recast layer. Some amorphous phase is also present. Findings indicate sub-surface pores between 10 nm and 200 nm diameter formed by gas expansion are observed. If the formation of such pores can be generalised for EDM processing of other materials, this phenomenon may contribute to the reduced mechanical integrity of such machined surfaces. Significant tool electrode material deposition with crystals of down to 3 nm diameter also occurred in the workpiece surface. The nano-scale of embedded material may have implications for the progress of electrical discharge machining as a coating process and the properties of such coatings.

© 2012 Elsevier B.V. All rights reserved.

## 1. Introduction

Electrical discharge machining (EDM) is a potential technique for the surface preparation and machining of the single crystal silicon ingot. High accuracy and lack of mechanical contact between tool and workpiece give it advantages over mechanical based cutting processes, particularly for brittle materials as such single crystal silicon. Silicon finds abundant applications in the semiconductor industry since its electrical properties can be precisely controlled. It is typically processed using lithographic techniques and chemical etching to introduce fine features, and the minimum feature size obtainable by lithography is fundamentally limited by the wavelength of the incident energy according to the Rayleigh criterion. As micro-EDM becomes ever capable of producing finer features, for example sub-1  $\mu\text{m}$  holes have now been achieved (Egashira et al., 2010), EDM is a potentially competing technology for the fabrication of some prototype components without the need for expensive lithographic tooling.

Slicing of single-crystal silicon by wire-EDM has been the subject of research in recent years. For example Takino et al. (2004) successfully cut low-resistivity silicon wafers, although some cracks and a rough surface were observed. Takino et al. (2005) further improved upon this by using a finishing operation to produce a crack-free surface, although in both cases cutting with oil produced a better finish than using a water dielectric. Kunieda and Ojima (2000) also improved the machining rate of sinking EDM for normal resistivity (8.3  $\Omega\text{ cm}$  n-type and 354  $\Omega\text{ cm}$  p-type) single crystal silicon by reducing the contact resistance between the workpiece and the metal clamping system by vacuum evaporation plating the contact surface with Al and Au-Sb for p and n-type wafers respectively.

Despite such interest in improving the machinability of silicon wafers by EDM, microstructural changes at the machined surface as well as any sub-surface defects induced by the process have not been investigated. This is of particular importance since defects such as cracks or pores, as well as amorphisation/re-crystallisation will influence the optical as well as electronic and mechanical performance of the wafers. Precision diamond machining, a potentially competing technology for the cutting of silicon, has been the subject of sub-surface characterisation. Yan et al. (2009) used TEM and Raman spectroscopy to characterise the surface damage of silicon after precision diamond machining. An amorphous layer

\* Corresponding author. Tel.: +44 7821988194.

E-mail addresses: [epxjm2@nottingham.ac.uk](mailto:epxjm2@nottingham.ac.uk) (J.W. Murray), [michael.fay@nottingham.ac.uk](mailto:michael.fay@nottingham.ac.uk) (M.W. Fay), [kunieda@edm.t.u-tokyo.ac.jp](mailto:kunieda@edm.t.u-tokyo.ac.jp) (M. Kunieda), [adam.clare@nottingham.ac.uk](mailto:adam.clare@nottingham.ac.uk) (A.T. Clare).

**Table 1**  
Properties of silicon workpiece.

Type	Dopant	Orientation	Resistivity ( $\Omega$ cm)	Thickness ( $\mu$ m)
n	Antimony	[100]	$\leq 0.02$	500

with fluctuating thickness is formed, with a dislocation rich region below this. The mechanical cutting regime in diamond-turning of single crystal silicon has also been investigated and despite the extreme brittleness of the material, a ductile cutting regime, producing spiral-like chips can be achieved under careful machining parameter selection (Chao et al., 2002). The EDM process however involves a distinct material removal mechanism which does not depend upon shear mechanics to remove material and the resulting surface damage is neither predictable nor understood.

Moreover, the analysis of a pure material workpiece such as single crystal silicon after EDM also allows a fundamental study of the movement of material from the dielectric, sub-surface inclusions, and the scale of any microstructures formed in the machined recast layer. The movement of material from tool electrode and from powder suspended in the dielectric onto the workpiece has gained considerable interest recently. Several authors have observed the movement of material between electrodes and the subsequent layer produced, such as by Marafona (2007) as well as Murray et al. (2012) both using EDX analysis, and this phenomenon has been proven as a novel coating method, for producing a TiC layer using a sacrificial titanium/graphite electrode (Hwang et al., 2010) and from Ti powder suspended in the dielectric (Janmanee and Muttamara, 2012). However, the microstructure of such coatings, and that of material embedded in the recast layer has not been examined in great detail. The only analysis at the sub-micron scale of the EDM'd surface has been conducted by Cusanelli et al. (2004) whereby ferritic steel was examined after machining. Significant carbon contamination at the surface was measured in this work along with martensitic and austenitic transformations; however, no tool electrode material was observed in the recast layer of the workpiece. The aims of this study are therefore two-fold. It aims to understand the damage induced in the surface of a single-crystal silicon ingot subject to electrical discharge machining, in order to accompany studies regarding machining rate and stability, and therefore promote EDM as feasible for the processing of the material. The second aim is to study the EDM induced surface by TEM in order to draw conclusions on the movement of material from the dielectric, as well as any defects at or near the surface. This study therefore is of significant interest for researchers involved in semi-conductor processing, as well as the wider EDM community.

## 2. Experimental

### 2.1. EDM and materials

Machining was performed using a Panasonic sinking-EDM with a rotating electrode for flushing of machined debris. A schematic of the set-up is shown in Fig. 1. A single polycrystalline Tungsten electrode with diameter  $150 \pm 5 \mu$ m was prepared using wire electrical discharge grinding (WEDG) (Masuzawa et al., 1985) before being sunk into the workpiece. The workpiece material for this study was an n type single-crystal silicon wafer, properties shown in Table 1. Open circuit voltage and capacitance of the relaxation type pulse generator remained constant at 90 V and 1000 pF respectively, and a kerosene oil dielectric was used.

Preliminary trials to acquire stable machining conditions involved the sinking of through holes (500  $\mu$ m) in the Silicon wafers. From these experiments it was observed that stable machining was only maintained before the hole depth reached

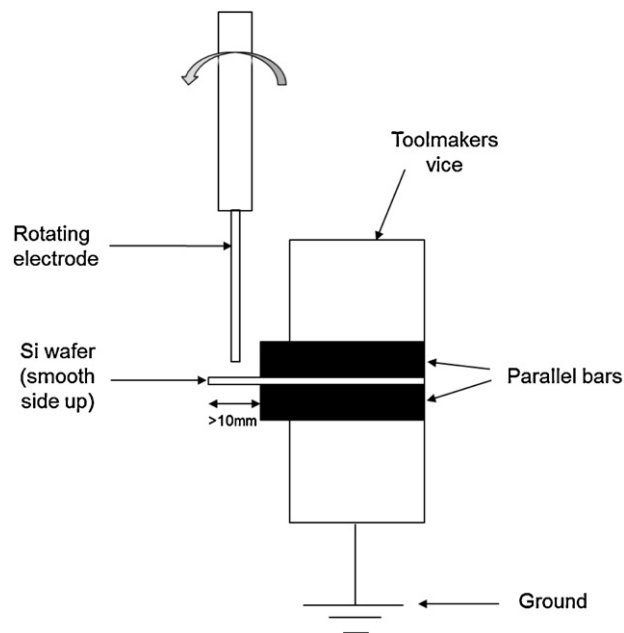


**Fig. 1.** Schematic of clamping arrangement.

100  $\mu$ m, corresponding to an aspect ratio (hole depth/diameter) of 1/1.5, beyond which an unstable regime took place. Beyond this hole depth, the electrode rotation flushing effect is not sufficient for the ejection of machined debris from the machining region and a build-up of detritus occurs, creating short circuit conditions and temporary cessation of machining, hence reducing material removal rate and inducing hole deformities. Based on this, the sinking of three 100  $\mu$ m-deep blind holes was performed. Tool electrode polarity was also set to positive as more stable conditions were observed for this arrangement. Current values during machining were measured by a current clamp and oscilloscope set-up. The mean peak current across the three machining experiments was 6.18 A with a standard deviation of 0.53 A. The mean machining time for each hole was 72.9 s.

### 2.2. TEM

Focused ion beam (FIB) machining using an FEI Quanta 200 3D FIBSEM was performed to prepare a lamellar from one of the machined holes. Given that it was not possible to perform a lift out from the bottom surface of the hole due to the restricted manipulator entry angle, an "L" shaped lamellar was prepared from the top edge of the hole. A micrograph of one of the machined holes, along with the site of lift-out and a TEM image of the lamellar attached to the copper grid are shown in Fig. 2.

TEM and Scanning TEM (STEM) were performed with a JEOL 2100F at 200 kV. Bright field (BF), Dark Field (DF), and High Angle Annular Dark Field (HAADF) STEM were performed using a JEOL Digital STEM System. Energy dispersive X-ray spectroscopy (EDX) mapping was performed in STEM mode using an Oxford Instruments INCA X-ray Microanalysis System.

### 2.3. Laser-Raman spectroscopy

Laser micro-Raman spectroscopy was performed using a LabRAM HR (Horiba) confocal Raman microscope with green 532 nm wavelength laser. An exposure time of 5 s was used for all measurements. The process is particularly useful for the rapid evaluation of the state of pure materials such as single-crystal. The maximum penetration depth of 532 nm laser in Silicon is 927 nm

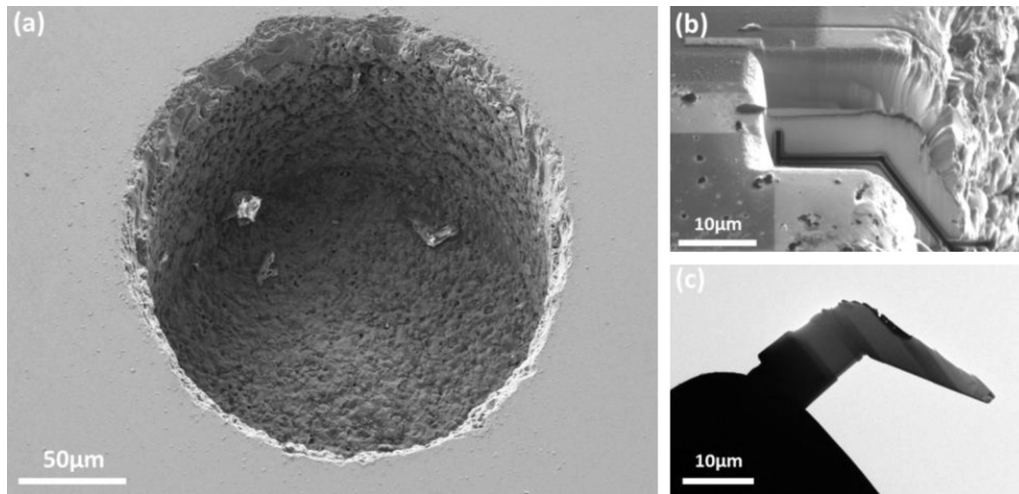


**Fig. 2.** (a) Machined hole on n[100] type Si wafer, machined with +ve electrode, (b) TEM lamellar position on edge of hole, (c) Thinned Lamellar attached to a Cu lift-out grid.

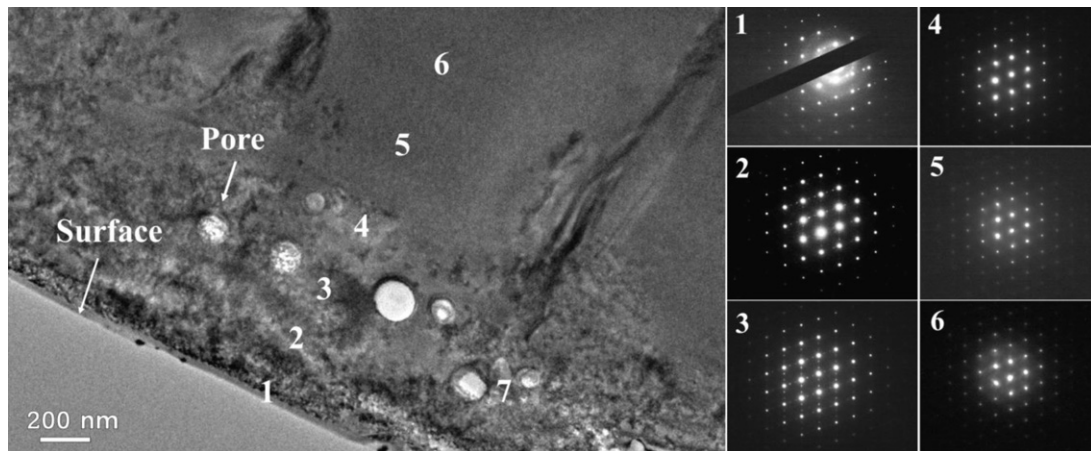


**Fig. 3.** Bright field TEM image of recast layer. Sub-surface bubbles are revealed. Diffraction patterns indicate some amorphicity in location 1, a twinned region in 2 and 3, and purely single crystal in locations 4, 5 and 6.

(Shibahara et al., 2005). This is important for qualifying the depth assessed by Raman spectroscopy and therefore whether its results represent the machining induced recast layer or a combination of it and the bulk beneath.

### 3. Results

#### 3.1. Microstructural changes and porosity

A sequence of selected area electron diffraction (SAED) patterns in a direction perpendicular to the machined surface and in intervals of approximately 250 nm was used to determine microstructural changes induced by the EDM process (Fig. 3). Close to the surface, in pattern 1, a combination of an amorphous structure and single crystal silicon pattern was identified. The broad width of the rings indicates amorphicity. In locations 2 and 3, amorphous signal was no longer present, and a combination of single crystal and a twinned pattern was observed, this phenomenon is further elucidated and discussed around Fig. 10. In locations 4, 5 and 6 a solely single crystal pattern, the same as that of a non-EDM'd region of the lamellar (see Fig. 10(a)) can be seen.

The lamellar was then tilted relative to the electron beam so that the direction of the beam was no longer perpendicular to a zone axis, thereby exposing any underlying amorphous or polycrystalline structure otherwise hidden against the dominant crystalline

pattern. An SAED pattern from location 2 after this process can be seen in Fig. 4. A combination of an amorphous structure (broad rings) and a fine polycrystalline signal (small points in fine rings) can be seen in this new pattern. This suggests that despite a strong crystalline pattern previously detected, the surface is also

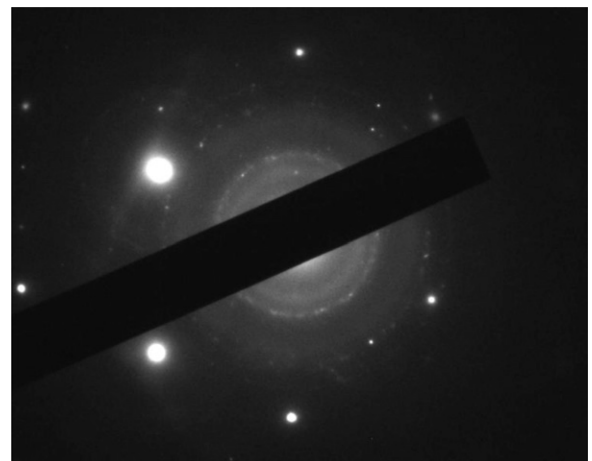


**Fig. 4.** Electron diffraction pattern from location 2 in Fig. 3 when beam is tilted away from the zone axis. A polycrystalline signal is observed.

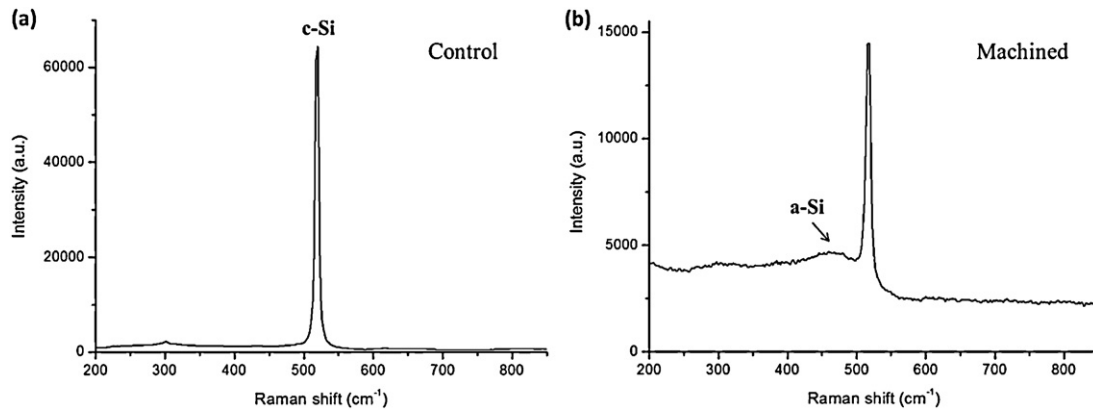


Fig. 5. Typical Raman spectra of (a) as-received silicon wafer and (b) bottom of machined hole.

composed of a fine nano-crystalline structure, since the diameter of the pattern region was about 150 nm, as well as an amorphous matrix.

Given that FIB machining to prepare a lamellar sometimes results in a thin region of amorphisation, laser-Raman spectroscopy was performed on the as-received silicon wafer as well as the surface of the original machined hole to confirm the presence of the amorphous layer after electrical discharge machining. Example Raman spectra from both the as-received single-crystal material and the machined surface can be seen in Fig. 5. A solitary sharp peak is observed for the single crystal material at  $520\text{ cm}^{-1}$ , consistent with that for c-Si (Zwick and Carles, 1993). A hump was observed on all spectra taken from the machined surface at approximately  $470\text{ cm}^{-1}$  Raman shift, consistent with an amorphous phase (Yan, 2004). Despite this, a large peak for c-Si still remained for all spectra taken from the machined surface. This supports the SAED patterns indicating crystalline silicon is the dominant structure with some amorphisation at the surface.

Pores beginning at 400 nm below the surface and terminating after  $1.1\text{ }\mu\text{m}$  were observed (see Fig. 3). The pores were observed up to the very edge of the observed recast layer. The smallest diameter of pore was approximately 10 nm with a maximum of 200 nm. The highly spherical shape seen at higher magnification suggests they are formed by either the expansion or contraction of gas trapped in the recast layer. A concentration of deposits was also observed at the outer rim of many of the pores, which could be explained by the agglomeration of particles at their edges as the molten recast layer containing particles flows around the trapped gas. If the circular nature of the pores is explained by the expansion of gas, then

particle concentration at their edges would also be explained by gas expansion forcing the particles outwards, where their motion is subsequently impeded by the presence of liquid matter. The high electron transparency of the pores, i.e. their brighter appearance in bright field imaging, also indicates the lamellar is much thinner in these regions (see Fig. 6).

### 3.2. Material deposition

A significant compositional change was observed in the machined surface. HAADF STEM imaging in particular revealing contrast according to atomic number indicated the presence of a heavier element in the surface (see Fig. 7), and this contamination was observed up to approximately  $1.2\text{ }\mu\text{m}$  depth into the surface. To prove the elemental composition of the surface, and to elucidate the polycrystalline selected area diffraction patterns, EDX analysis was performed.

Fig. 7 shows HAADF STEM images of nano-particles of a heavier element in the recast layer of the workpiece. The region mapped by EDX is indicated, and the W map shows Tungsten matching the positions of the particles in the micrograph. The Si map also shows the matrix is Silicon. This suggests that tool electrode material from the dielectric is mixed in with the discharge melt pool and makes a significant contribution to the composition of the machined surface. A Carbon map is also shown, with a distribution more uniform than that of the Tungsten deposits, but also with some regions of localised concentration. Bright field TEM imaging (see Fig. 8) was used to observe size, shape and crystal orientation of the tungsten particles.

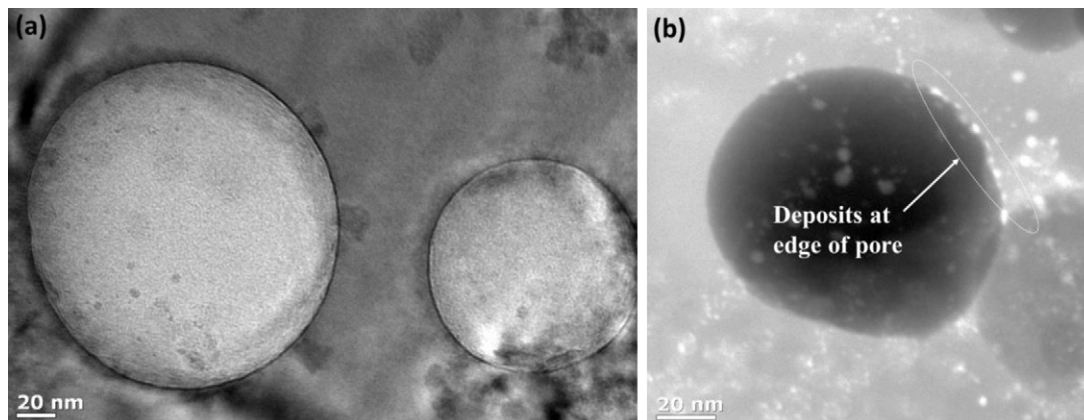
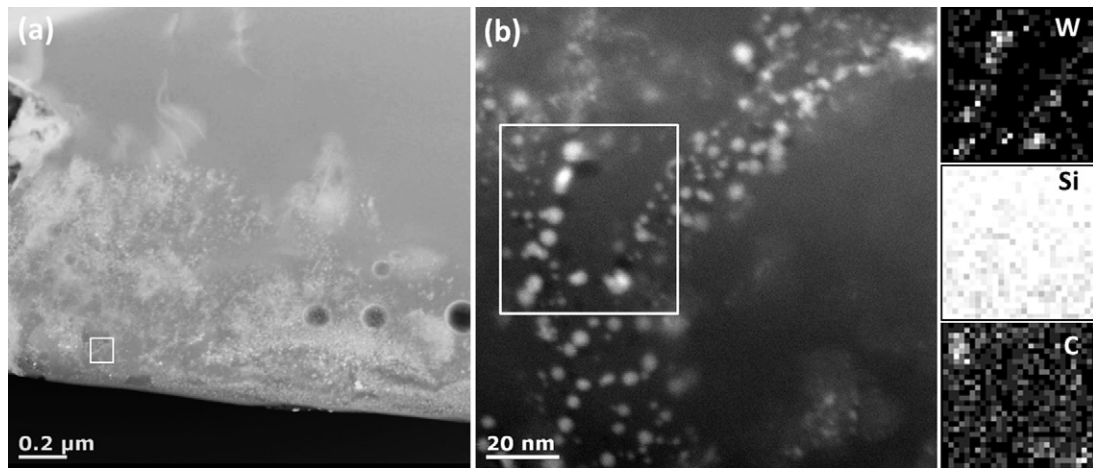


Fig. 6. Pores imaged in (a) Bright field TEM and (b) Dark field STEM. High electron transparency is observed. Gas expansion may be responsible for the movement of deposits to the edge of the pores. Overlapping pores at different depths can also be seen in (b).



**Fig. 7.** HAADF STEM image of deposits in recast layer with indicated EDX region with Tungsten, Silicon and Carbon EDX maps proving absorption of tool electrode material and Carbon into the silicon recast layer.

A defined crystal structure can be seen in the location of particles, whereas a distinct amorphous matrix with no lattice structure can be observed for the surrounding silicon. The crystalline lattice structure of silicon shown in Fig. 11 can be used for a comparison under high resolution imaging to the amorphous structure seen in Fig. 8. The smallest size of tungsten crystal observed was approximately 3 nm. It was also observed that the lattices of the tungsten crystals were randomly oriented, this may be explained by their movement into the surfaces as solid particles and their crystal structure is maintained, and therefore crystal growth by a directional cooling gradient was unlikely to be responsible for their formation.

### 3.3. Dislocations and strain

Below the recast layer characterised by high tool deposition and pores, an inhomogenous dislocation rich region was observed (Fig. 9(b)). Contrast arises from dislocations in BFTEM mode since in these locations the lattice is distorted and more electrons will satisfy the specific Bragg diffraction angle in these locations compared to the rest of the single crystal sample where the image is formed (i.e. brighter contrast regions) by the admittance of the primary (non-diffracted) beam, hence darker contrast is observed in dislocation regions in BFTEM mode. This TEM imaging principle also shows the polycrystalline regions near the surface in Fig. 9(a), since a mixture of light and dark contrast is observed, suggesting randomised

orientation. In Fig. 9(a), bend contours can also be seen in the single crystal region of the lamellar beneath the recast layer typical of a single crystal when the lamellar is slightly buckled, whereas in the contaminated recast layer at the surface, such contours cannot be easily identified. This effect clearly distinguishes the boundary of the recast layer. Lattice strain can be inferred by the presence of contrast fringes observed in BFTEM mode. In Fig. 9(c) localised contrast fringes can be seen in a region just beneath the recast layer, inferring the presence of a defect. In the vicinity of a defect such as a dislocation, it is known that the diffraction planes are distorted. This strain field around a dislocation core is sufficient to locally tilt lattice planes into and out of the Bragg condition, thereby resulting in an oscillation of intensity of the outgoing beam, producing contrast fringes (Williams and Carter, 1996).

## 4. Discussion

### 4.1. Amorphisation and porosity

Based upon TEM imaging as well as diffraction patterns, the machined surface of single crystal silicon is modified from that of the bulk crystal. Pores of a range of sizes from 10 nm to 200 nm comprise the recast layer. Since little TEM work has been done on the analysis of the recast layer of EDM'd materials, this is the first observation of sub-micron sized voids in the machined surface. Diffraction patterns and direct imaging of the lattice have exposed that the surface is composed of a mixture of amorphised and twinned crystalline silicon.

TEM selected area electron diffraction patterns of a sequence of regions of the recast layer when the electron beam was perpendicular to the zone axis showed a clear single crystal silicon pattern was present in all regions. In combination with single crystal silicon, nearest the surface an amorphous region was identified based on these patterns, and beneath this a twinned region was identified. Approximately 800 nm into the machined surface, a twinned pattern was no longer observed and a single crystal silicon pattern equal to that of the non-machined section of the lamellar was seen. After the beam was tilted away from the zone axis, a polycrystalline pattern emerged on amorphous rings in location 2 in Fig. 3. High resolution imaging of the surface as well as Raman spectroscopy of the machined surface also confirmed that a combination of twinning and amorphisation is the damage mechanism occurring when machining single-crystal silicon with EDM. This is in contrast to a solely amorphous layer which has been shown to

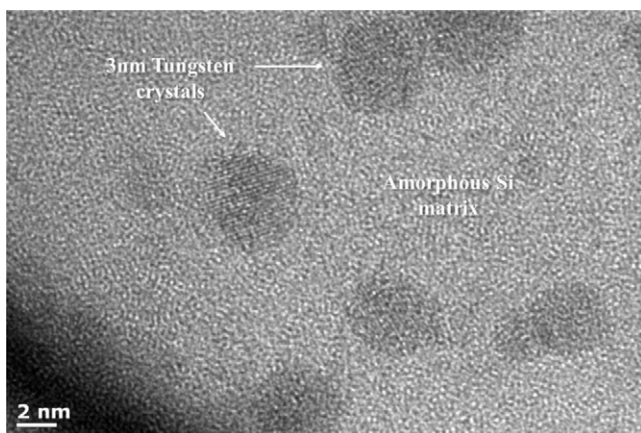


**Fig. 8.** Tungsten crystals of approximately 3 nm diameter in an amorphous region of silicon.

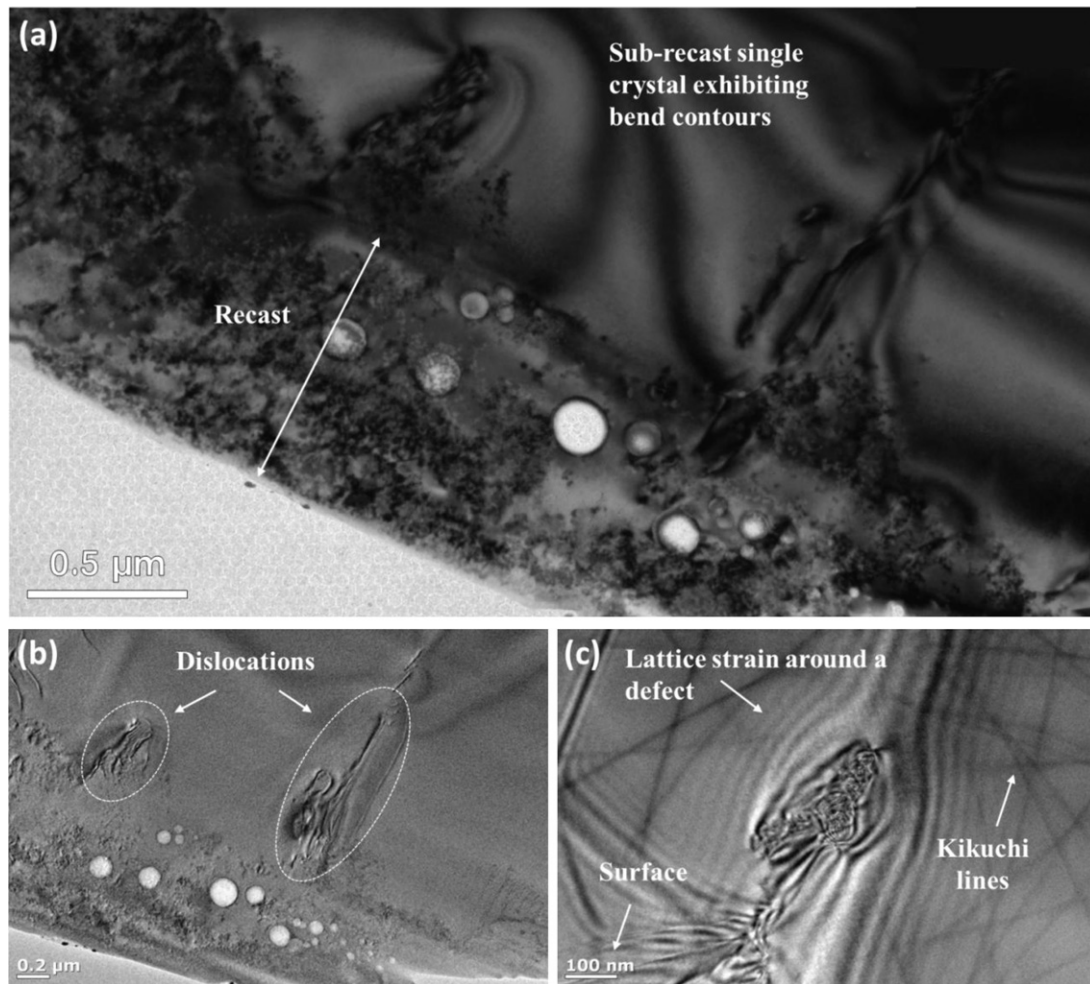


**Fig. 9.** (a) Bright-field TEM image showing extent of recast layer and single crystal region beneath showing bend contours, (b) BFTEM image of the same area showing dislocation regions (c) BFTEM image of strain field induced by a dislocation.

occur after machining single crystal silicon by mechanical means in the ductile cutting mode.

Under ductile mechanical cutting conditions as have been achieved by several authors a purely amorphous layer is observed, for example by Fang et al. (2007) using TEM diffraction patterns of amorphous machined chips, and by Yan et al. (2009) using Raman spectroscopy and direct TEM observation. Under brittle machining conditions, a polycrystalline pattern in an amorphous matrix is seen (Fang et al., 2007). After EDM machining from our results, amorphous regions are present only in combination with a crystalline matrix. To eliminate the factor of the FIB amorphisation during preparation of the lamellar, Raman spectroscopy confirmed the presence of the amorphous phase in the machined surface with the characteristic hump in the signal, peaking at approximately  $470\text{ cm}^{-1}$ . The maximum penetration depth of 532 nm laser in silicon is 927 nm (Shibahara et al., 2005). It is also important to note that the Raman shifts recorded represent an average value from the entire scattering volume between the surface and the 927 nm maximum depth. Combined with the observation of deposition of material up to approximately  $1.2\text{ }\mu\text{m}$  into the surface, it is reasonable to suggest the Raman shifts observed represent only the recast layer and not the bulk beneath. Therefore the strong Raman shift for c-Si at  $520\text{ cm}^{-1}$  as well as the amorphous hump in Fig. 5(b) supports the findings from the SAED patterns that the recast layer is not a uniform region of the amorphous phase but is only partially amorphised. A polycrystalline SAED pattern was also observed  $250\text{ nm}$  from the surface after tilting the beam away from the zone axis,

and upon EDX analysis, HAADF imaging and direct observation of the nano-crystals in the surface it was concluded that this pattern arises from the deposition of crystals into the recast layer from the tool electrode, although this was not in sufficient enough quantity to noticeably affect the Raman spectrum.

#### 4.2. Twinning

Crystal twinning is when two or more crystals are formed in a symmetrical fashion. This means that lattice points in one crystal are reflected in the twinned crystal by a twin plane (or mirror plane) in the lattice. Twinning can occur either during growth of a crystal, or if a crystal is subjected to stress. In several SAED patterns of our machined surface, a strong twinning pattern of the single crystal silicon matrix was observed. Fig. 10 compares an SAED pattern of a non-machined region of the single crystal lamellar with a pattern from location 7 in Fig. 3. In (a) lattice points are identified, and in (b) the lattice planes across which the crystal twins are mirrored can be seen. Two twins were identified according to the patterns, one is a twin of the parent matrix mirrored along the  $(1\ 1\ \bar{1})$  plane and the other is a twin of the parent matrix along the  $(1\ 1\ 1)$  plane. Lattice points and planes were identified according to previous work on twinning during semiconductor growth (Sarney, 2003). A schematic is also shown to illustrate more clearly the twin planes about which the crystal is mirrored.

There is evidence that impurities, especially carbon promote twinning during growth of crystalline silicon (Duffar and Nadri,

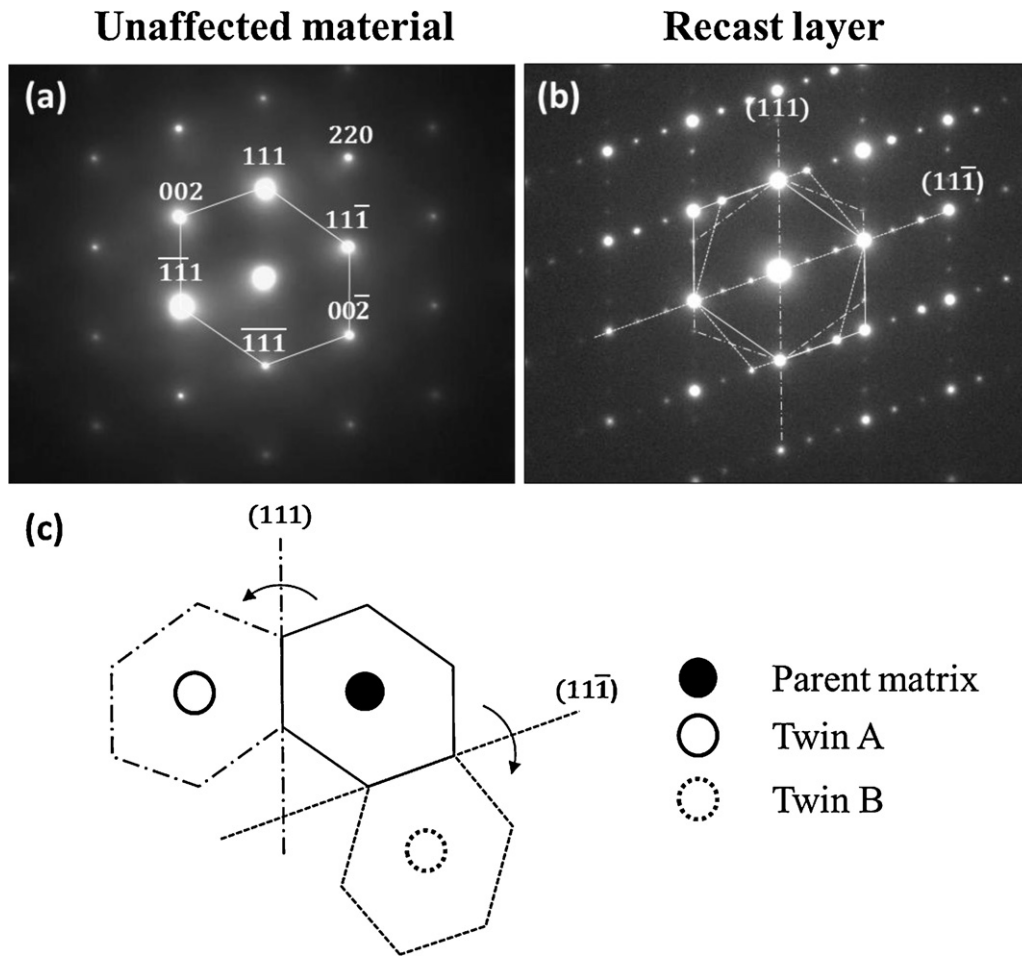


**Fig. 10.** Diffraction patterns from (a) location on lamellar not subject to machining, revealing single crystal silicon structure (b) location “7” on Fig. 3 revealing twin structure (c) schematic of twinning planes.

2010). Since it is understood that the machined surface is molten during spark on-time, and the observation of pores in our results supports this, it can be concluded that twin formation in this study likely occurred as a result of crystal growth during resolidification, and since carbon as well as tungsten contamination has been detected in our EDX results, the presence of these contaminants may explain the interruption of crystal growth and the subsequent formation of twins. Given the primary lattice structure (i.e. the brightest spots) of the recast layer seen in the diffraction pattern in Fig. 10(b) is the same as that of the unaffected, single crystal structure of the lamellar in Fig. 10(a), this would suggest that epitaxial growth of silicon is occurring, whereby a crystalline structure in the recast layer is grown beginning at the liquid–solid interface and is a continuation of the bulk crystal structure, although in this case twinning was observed to occur during crystal growth. Treatment of the mechanically machined surface of single-crystal silicon has been the subject of research in order to eliminate the amorphous damaged structure and recreate the crystalline structure beneath by epitaxial growth. For example Yan et al. (2007) successfully reconstructed the bulk single crystal structure in the surface of a machining-damaged silicon wafer by the use of nanosecond pulsed laser irradiation surface treatment. This research has shown that cutting by EDM may be a competing technology for maintaining crystal quality in single-crystal silicon wafers.

The presence of twins in the recast layer was also confirmed by direct BFTEM imaging of the lattice. Fig. 11 shows a TEM image of a twin in the parent silicon matrix, with twin boundaries clearly visible.

#### 4.3. Material deposition

EDM is fundamentally different from mechanical machining techniques in that the mechanism of material removal depends on the superheating of the molten workpiece and the subsequent pressure drop at the end of spark duration expelling some of the melt pool into the dielectric. Despite the use of a flowing

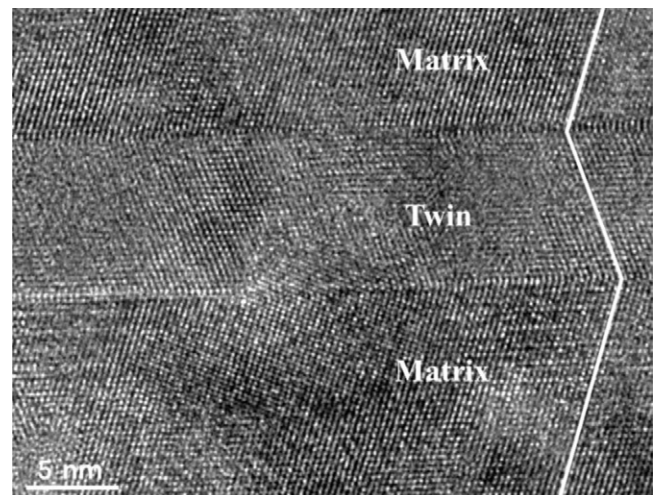


**Fig. 11.** Twin observed approximately 100 nm from the surface of the sample.

dielectric to remove this resolidified debris from the machining region and maintain predictable electrical conditions in the spark gap, carbon from oil based dielectrics is known to move during machining into the surface of the workpiece (Cusanelli et al., 2004) and the tool electrode (Kunieda and Kobayashi, 2004). This is thought to occur due to thermal dissociation or “cracking” of the carbon based oil (Mohri et al., 1995). In EDX results in order to identify the foreign particles, carbon was also detected in the recast layer, in a more uniform distribution than the tungsten deposits, supporting the notion that carbon moves gradually into the molten surface from the dielectric, and not deposited as larger debris particles.

Also, of importance, is the movement of the tool electrode material into the surface of the workpiece. Accretion of the tool electrode material onto the workpiece during EDM has been achieved by several researchers, such as Mohri et al. (1993) using a composite structured electrode onto a steel workpiece, as well as by Ho et al. (2007) onto Ti-6Al-4V and proposed as a practical method of introducing coatings onto tools such as drills (Moro et al., 2004). Yang et al. (2010) simulated the movement of atoms from both electrodes at the end of discharge, and found that both single atoms and clusters of atoms can attach to the top surfaces of the opposite electrodes. This mechanism of attachment however would not explain the mixture of a considerable amount of opposite electrode within the entire thickness of the recast layer, as observed in this study. It has also been shown (Murray et al., 2012) that a mechanism of attachment of material onto electrodes is the remelting of debris in the dielectric by the secondary discharge process, thereby lodging previously removed material onto the melt pool on the opposite electrode. This remelting process may explain the movement and attachment of a large amount of tool material on the workpiece. The nano-scale diameter of embedded tool electrode (tungsten) crystals observed in the recast layer is of particular interest from the perspective of EDM coatings, since a nano-structured layer of deposited material would have significant benefits for the mechanical/thermal properties of the coating. Recent work on electrical discharge coating (EDC) has shown that titanium deposition from powder suspension onto a tungsten carbide substrate can increase surface hardness to 1750HV from 990HV in the substrate (Janmanee and Muttamara, 2012). Despite this no microstructural characterisation was performed on the coating to explain the mechanical properties. It is possible that the nano-scale crystals observed in our experiments are also present after such electrical discharge coating processes. Future work is necessary to characterise the microstructure of such coatings and therefore determine if the nano-scale microstructure also occurs during this process.

#### 4.4. Deformation

Dislocation regions were observed just beneath the recast layer, where pores and tool electrode contamination were no longer observed. These regions of dislocations were not homogenous but in regions of concentrations. It is proposed that the cooling gradient and the subsequent stress induced by the sparking process result in the compensation of this stress in the solid bulk just beneath the melt pool by the nucleation of dislocations. Since the workpiece is single crystal and has no grain boundaries, the propagation of dislocations across the whole width of the lamellar, or the creation of dislocation loops, occurred and can be observed. The damage observed in this study in silicon is similar to that observed by Yan et al. (2009) in precision diamond machining, whereby an amorphous layer is created nearest the surface with a dislocation-rich region beneath this.

## 5. Conclusions

- A fundamental study on the surface of EDM'd single-crystal silicon has been for the first time performed.
- Two phenomena at the nano-scale created by the EDM process have been observed not before discussed in literature: nano-scale pores and nano-crystals of embedded tool material. Both of these have implications for the creation of coatings by the electrical discharge process.
- Spherical pores between 10 nm and 200 nm diameter were observed in the machined surface, generated by the absorption of gas in the surface when molten.
- Electron diffraction patterns and laser-Raman spectroscopy were used to show that the surface microstructure is primarily twinned-crystalline with some amorphous silicon. The twinned-crystalline structure is formed due to epitaxial growth during resolidification of the molten surface.
- Significant movement of tool electrode material (tungsten), as well as carbon from the dielectric into the machined surface occurs during machining.
- The size of embedded tungsten particles is typically several nm with the smallest particles approximately 3 nm in diameter. The particles were observed in random orientations in the recast layer.
- These new structures observed at the nano-scale of an EDM'd workpiece have implications for the integrity of components subject to the machining process, and TEM analysis should be considered for future analysis of EDM recast layers.

## References

- Chao, C.L., Ma, K.J., Liu, D.S., Bai, C.Y., Shy, T.L., 2002. Ductile behaviour in single-point diamond-turning of single-crystal silicon. *Journal of Materials Processing Technology* 127, 187–190.
- Cusanelli, G., Hessler-Wyser, A., Bobard, F., Demellayer, R., Perez, R., Flükiger, R., 2004. Microstructure at submicron scale of the white layer produced by EDM technique. *Journal of Materials Processing Technology* 149, 289–295.
- Duffar, T., Nadri, A., 2010. On the twinning occurrence in bulk semiconductor crystal growth. *Scripta Materialia* 62, 955–960.
- Egashira, K., Morita, Y., Hattori, Y., 2010. Electrical discharge machining of submicron holes using ultrasmall-diameter electrodes. *Precision Engineering* 34, 139–144.
- Fang, F.Z., Wu, H., Zhou, W., Hu, X.T., 2007. A study on mechanism of nano-cutting single crystal silicon. *Journal of Materials Processing Technology* 184, 407–410.
- Ho, S.K., Aspinwall, D.K., Voice, W., 2007. Use of powder metallurgy (PM) compacted electrodes for electrical discharge surface alloying/modification of Ti-6Al-4V alloy. *Journal of Materials Processing Technology* 191, 123–126.
- Hwang, Y.-L., Kuo, C.-L., Hwang, S.-F., 2010. The coating of TiC layer on the surface of nickel by electric discharge coating (EDC) with a multi-layer electrode. *Journal of Materials Processing Technology* 210, 642–652.
- Janmanee, P., Muttamara, A., 2012. Surface modification of tungsten carbide by electrical discharge coating (EDC) using a titanium powder suspension. *Applied Surface Science* 258, 7255–7265.
- Kunieda, M., Kobayashi, T., 2004. Clarifying mechanism of determining tool electrode wear ratio in EDM using spectroscopic measurement of vapor density. *Journal of Materials Processing Technology* 149, 284–288.
- Kunieda, M., Ojima, S., 2000. Improvement of EDM efficiency of silicon single crystal through ohmic contact. *Precision Engineering* 24, 185–190.
- Marafona, J., 2007. Black layer characterisation and electrode wear ratio in electrical discharge machining (EDM). *Journal of Materials Processing Technology* 184, 27–31.
- Masuzawa, T., Fujino, M., Kobayashi, K., Suzuki, T., Kinoshita, N., 1985. Wire electro-discharge grinding for micro-machining. *CIRP Annals – Manufacturing Technology* 34, 431–434.
- Mohri, N., Saito, N., Tsunekawa, Y., Kinoshita, N., 1993. Metal surface modification by electrical discharge machining with composite electrode. *CIRP Annals – Manufacturing Technology* 42, 219–222.
- Mohri, N., Suzuki, M., Furuya, M., Saito, N., Kobayashi, A., 1995. Electrode wear process in electrical discharge machining. *CIRP Annals – Manufacturing Technology* 44, 165–168.
- Moro, T., Mohri, N., Otsubo, H., Goto, A., Saito, N., 2004. Study on the surface modification system with electrical discharge machine in the practical usage. *Journal of Materials Processing Technology* 149, 65–70.
- Murray, J., Zdebski, D., Clare, A.T., 2012. Workpiece debris deposition on tool electrodes and secondary discharge phenomena in micro-EDM. *Journal of Materials Processing Technology* 212, 1537–1547.

- Sarney, W.L., 2003. Understanding Transmission Electron Microscopy Diffraction Patterns Obtained from Infrared Semiconductor Materials. Army Research Laboratory, Adelphi, MD.
- Shibahara, K., Matsuno, A., Takii, E., Eto, T., 2005. Green laser annealing with light absorber. In: 13th IEEE International Conference on Advanced Thermal Processing of Semiconductors, RTP 2005, pp. 101–104, art. no. 1613689.
- Takino, H., Ichinohe, T., Tanimoto, K., Yamaguchi, S., Nomura, K., Kunieda, M., 2004. Cutting of polished single-crystal silicon by wire electrical discharge machining. *Precision Engineering* 28, 314–319.
- Takino, H., Ichinohe, T., Tanimoto, K., Yamaguchi, S., Nomura, K., Kunieda, M., 2005. High-quality cutting of polished single-crystal silicon by wire electrical discharge machining. *Precision Engineering* 29, 423–430.
- Williams, D.B., Carter, C.B., 1996. *Transmission Electron Microscopy: A Textbook for Materials Science*. Springer, US.
- Yan, J., 2004. Laser micro-Raman spectroscopy of single-point diamond machined silicon substrates. *Journal of Applied Physics* 95, 2094–2101.
- Yan, J., Asami, T., Harada, H., Kuriyagawa, T., 2009. Fundamental investigation of subsurface damage in single crystalline silicon caused by diamond machining. *Precision Engineering* 33, 378–386.
- Yan, J., Asami, T., Kuriyagawa, T., 2007. Response of machining-damaged single-crystalline silicon wafers to nanosecond pulsed laser irradiation. *Semiconductor Science and Technology* 22, 392–395.
- Yang, X., Guo, J., Chen, X., Kunieda, M., 2010. Molecular dynamics simulation of the material removal mechanism in micro-EDM. *Precision Engineering* 35, 51–57.
- Zwick, A., Carles, R., 1993. Multiple-order Raman scattering in crystalline and amorphous silicon. *Physical Review B* 48, 6024–6032.